Journal of Biomedical Optics

SPIEDigitalLibrary.org/jbo

Evaluation and quantification of spectral information in tissue by confocal microscopy

Ulf Maeder
Kay Marquardt
Sebastian Beer
Thorsten Bergmann
Thomas Schmidts
Johannes T. Heverhagen
Klemens Zink
Frank Runkel
Martin Fiebich

SPIE

Evaluation and quantification of spectral information in tissue by confocal microscopy

Ulf Maeder,[a] Kay Marquardt,[b] Sebastian Beer,[a] Thorsten Bergmann,[a] Thomas Schmidts,[b] Johannes T. Heverhagen,[c] Klemens Zink,[a] Frank Runkel,[b] and Martin Fiebich[a]
[a]Technische Hochschule Mittelhessen—University of Applied Sciences, Institute of Medical Physics and Radiation Protection, Wiesenstraße 14, 35390 Gießen, Germany
[b]Technische Hochschule Mittelhessen—University of Applied Sciences, Institute of Bioprocess Engineering and Pharmaceutical Technology, Wiesenstraße 14, 35390 Gießen, Germany
[c]Inselspital, University Hospital, Institute of Diagnostic, Interventional and Pediatric Radiology, Bern, Switzerland

Abstract. A confocal imaging and image processing scheme is introduced to visualize and evaluate the spatial distribution of spectral information in tissue. The image data are recorded using a confocal laser-scanning microscope equipped with a detection unit that provides high spectral resolution. The processing scheme is based on spectral data, is less error-prone than intensity-based visualization and evaluation methods, and provides quantitative information on the composition of the sample. The method is tested and validated in the context of the development of dermal drug delivery systems, introducing a quantitative uptake indicator to compare the performances of different delivery systems is introduced. A drug penetration study was performed *in vitro*. The results show that the method is able to detect, visualize and measure spectral information in tissue. In the penetration study, uptake efficiencies of different experiment setups could be discriminated and quantitatively described. The developed uptake indicator is a step towards a quantitative assessment and, in a more general view apart from pharmaceutical research, provides valuable information on tissue composition. It can potentially be used for clinical *in vitro* and *in vivo* applications. [DOI: 10.1117/1.JBO.17.10.106011]

Keywords: spectral imaging; skin visualization; drug delivery; skin penetration study; confocal microscopy; quantitative uptake indicator.

Paper 12276 received May 3, 2012; revised manuscript received Jul. 19, 2012; accepted for publication Sep. 7, 2012; published online Oct. 1, 2012.

1 Introduction

The visualization of intrinsic and extrinsic substances in biological tissue is a very common task in the area of biomedical imaging. Fluorescence microscopy is a widely used technique to assess the local distribution of either intrinsic autofluorescent structures or incorporated fluorescent molecules. In the field of investigating drug delivery into biological tissue, especially skin tissue, fluorescent dyes are utilized in many cases as model agents. Amongst other techniques confocal,[1] multiphoton[2–5] and widefield[6] microscopy is used to evaluate pharmaceutical transdermal and dermal delivery systems.[7–9] Amongst others, highly potent approaches for delivery and therapy are microemulsion[10–12] and nanoparticle[13] formulations. Transdermal delivery systems are used for systemic drug distribution. Therefore the amount that permeated through the skin is of interest. *In vivo* studies commonly analyze the drug concentration in blood while *in vitro* studies, for example, have to analyze the concentration in equivalent receptor fluids. The drug concentration is normally determined by enzyme-linked immunosorbent assay (ELISA) or high-performance liquid chromatography (HPLC). The focus of dermal delivery systems is the penetration of drugs into the skin layers. An important parameter that can be assessed microscopically using vertical slices of the tissue is the penetration depth. The origin of tissues can be from excised skin addressing *in vitro* studies or in case of *in vivo* studies from skin biopsies. However, elaborated approaches using tape-stripping and HPLC analysis are often used for evaluation. HPLC analysis allows quantification of the drug in the whole sample without showing the distribution. Microscopy on the other hand shows the pathways of the transport but lacks the possibility to quantify without further calibration efforts.[1]

Microscopic tissue imaging is very promising in terms of identifying pathways and providing further inside in penetration processes. However, a major problem is that tissue often shows strong autofluorescence. Especially skin is very complex and consists of various endogenous fluorophores, such as melanin, elastin, riboflavin and NAD(P)H[2] and possesses a broad autofluorescence spectrum that may interfere with incorporated external dyes. Due to the overlapping spectra, the origin of the fluorescence in microscopic images cannot be easily distinguished by signal intensity alone. Recording spectral information along with intensity images would help in the identification. Some approaches for recording spectral information by means of hyperspectral setups can be found in the literature.

Previous studies describe the penetration of fluorophores into skin, skin tumor and irradiation investigations and the assessment of bruised and traumatic skin injuries.[14–19] Numerous further reports on spectral imaging that do not cover skin research are available.[20–24]

In this work we present a new confocal imaging approach with microscopic spatial resolution to visualize spectral information in tissue. The appropriate image processing steps based on normalized cross-correlation and the derivation of a new

Address all correspondence to: Ulf Maeder, Technische Hochschule Mittelhessen—University of Applied Sciences, Institute of Medical Physics and Radiation Protection, Wiesenstraße 14, 35390 Gießen, Germany. Tel: ++49 641 3092675; Fax: ++49 641 3092977; E-mail: ulf.maeder@kmub.thm.de

0091-3286/2012/$25.00

quantitative measure is described. The method is tested in the context of pharmaceutical development of drug delivery systems. In this study it is used to localize and evaluate fluorescent dyes in vertical slices of excised porcine skin to quantify uptake efficiency of a submicron emulsion for dermal transport. Although the method is discussed in the field of pharmaceutics, the method can be useful in more general applications in life-science imaging. Therefore, in addition to the presented *in vitro* considerations, potential *in vivo* applications are discussed.

2 Material and Methods

2.1 *Fluorescent Probe and Skin Autofluorescence*

Nile Red (Sigma-Aldrich, Germany) was used as a lipophilic fluorescent dye in the prepared submicron emulsion. The fluorescence spectrum of Nile Red remains stable over a wide pH range while influenced by the polarity of its solvents.[25] Figure 1 shows the emissions spectra of the dye, solved in 70% ethanol, in comparison to natural porcine skin measured by the confocal laser-scanning microscope. Nile Red has an emission peak at 580 nm excited with the 476 nm line of an argon laser. The broad autofluorescence spectrum of skin exists due to the numerous intrinsic fluorophores.

2.2 *Drug Delivery System Preparation*

Submicron emulsions were chosen as a delivery system because they have shown to enhance the penetration of substances into skin due to their particle size and surfactants.[26] Submicron emulsions are oil-in-water emulsions with a droplet size below one micrometer. It is a kinetic stable emulsion in which the droplet size is achieved by an incorporation of emulsifiers.[27] The oil phase consisted of oleth-3, -10, ethyloleat (Croda, Germany), coco-caprylat/caprat, cetearyl isononanoat (Cognis, Germany) and 0.002% Nile Red, while the aqueous phase consisted of sodium chloride, citric acid, potassium sorbate (Fagron, Germany), magnesium sulfate and glycerol (Caelo, Germany). The surfactant concentration was adjusted to achieve a hydrophilic-lipophilic balance value of 11. All ingredients obtained were of pharmaceutical grade. The physico-chemical properties were recorded to characterize the delivery system. The dynamic light scattering analyzing method (Zetasizer Nano ZS 90, Malvern Instruments, UK) showed a z-average size of 258 ± 3 nm with a polydispersity index of 0.16 ± 0.01. The viscosity of 2.4 ± 0.2 mPa · s was determined by RheoStress 300 Rheometer (ThermoHaake, Germany). Due to the preservation with potassium sorbate, the pH value was adjusted to 4.8 ± 0.2.

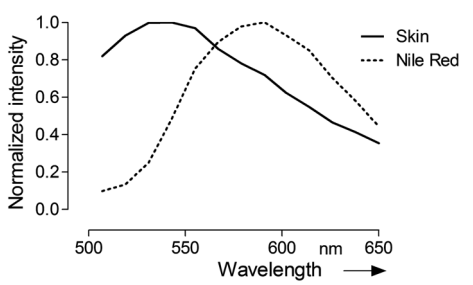

Fig. 1 Emission spectra of untreated porcine skin and the fluorescent dye Nile Red (Excitation: 476 nm). The spectral data was measured using the confocal microscope. The normalized presentation of the data shows the distinguishable emission peaks and the spectral overlap.

2.3 *Porcine Skin Samples*

Porcine ear skin is quite similar to human skin and was therefore used in this study.[28] Fresh ears of domestic pigs were obtained from a local abattoir and kept on ice during transport to the laboratory. After slaughtering, porcine ears were cleaned with water and shaved to remove the bristles. The full thickness skin was displaced with a scalpel and stored at −20 °C for less than three months.

Two preparation methods were used to obtain reference skin samples for validation measurements and penetration skin samples. The latter were used for the penetration study that evaluates delivery system performance.

2.4 *Reference Skin Samples*

The frozen skin specimens were cut into 10-μm thick slices using a cryo-microtom (Leica Microsystems, Germany) and then transferred into 70% ethanol with different Nile Red concentrations for 10 min. The dye was soaked up and excessive dye was removed from the skin under flowing water. The dye concentrations (0.2, 1, and 2 µg/mL) were chosen to cover a common recovery range of agents in the specimens of drug penetration studies. These reference skin samples were used to derive the sensitivity of the imaging scheme.

2.5 *Penetration Skin Samples*

The penetration of Nile Red into skin was performed on a Franz diffusion cell setup. On the day of experiment the frozen skin was thawed and fixed between the donor and receptor chamber of the Franz diffusion cell (Gauer Glas, Puettlingen, Germany). The penetration area had a diameter of 1.767 cm^2 and was in contact to 12 mL phosphate buffered saline (PBS) temperatured to 32.5 °C on the dermis side. The submicron emulsion was applied as infinite-dose (300 μL) for 3 h, 6 h, 8 h and 24 h to three porcine skin samples each to get a total of 12 experiment samples. After each time period, the skin was removed from the diffusion cell, wiped and washed with 50 mL aqua dest. The specimen was mounted into a freezing medium (Leica, Germany), shock frozen by fluid nitrogen and cut into various 10 μm thick vertical slices in order to prepare penetration samples for microscopy.

2.6 *Spectral Imaging*

Spectral imaging was performed using a TCS SP5 confocal laser-scanning microscope (Leica Microsystems, Mannheim, Germany) equipped with a detection unit that allows spectral discrimination to selectively detect narrow wavelength bands. The recorded fluorescence emission region (excitation at 476 nm) starting at 495 nm up to 650 nm (divided into 10 single detection bands that are 20 nm wide) was chosen to cover the spectra of porcine skin and Nile Red. A 0.7 NA water immersion objective (20×) was used and the image resolution was set to 512×512 pixel with a pixel size of 1.51 μm^2, resulting in a field of view of 775×775 μm^2. The generated image stacks were of the dimensions $xy\lambda$. The reference spectrum of Nile Red was recorded in the same way. Figures 2 and 3 give an overview of a 24 h penetration sample in comparison to natural (untreated) skin. The series of λ-stack pictures and an exemplary spectrum of the selected regions of interest (ROI) are shown to illustrate the different spectra. These spectral differences are used for the image processing scheme.

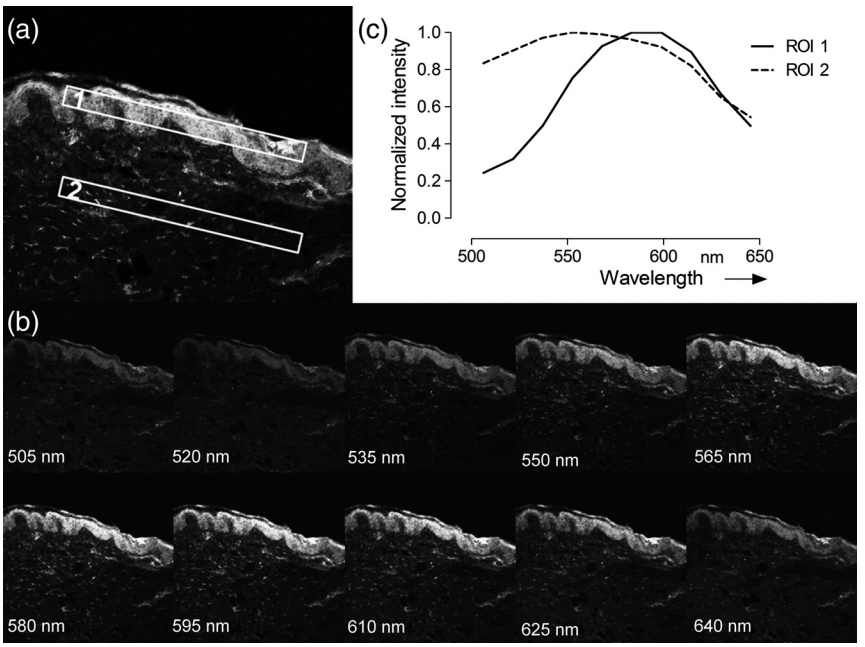

Fig. 2 Overview (a), images of the λ-stack (b) and spectra of ROI 1 and 2 (c) of a 24 h penetration skin sample. The given wavelengths of the λ-stack describe the center of the 20 nm wide wavebands.

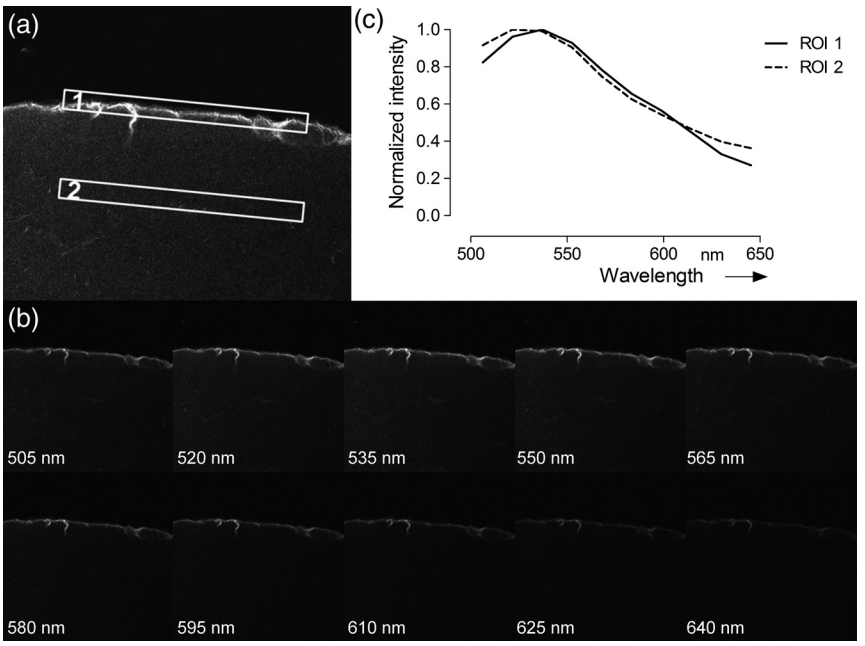

Fig. 3 Overview (a), images of the λ-Stack, (b) spectra of ROI 1 and 2, (c) of an untreated skin sample. The given wavelengths of the λ-stack describe the center of the 20 nm wide wavebands.

2.7 *Image Processing Scheme*

The image processing starts with the application of a threshold to exclude pixels with low intensities. The background or noisy image regions are excluded from the calculations. In the next step, the intensity data are normalized along the λ-axis to calculate intensity independent spectra for each image pixel. The normalized cross correlation (CC) metric is used to quantify the similarity between the normalized sample spectra and the reference spectra of Nile Red.

$$CC = \frac{\sum [S_{Ref}(i) - \bar{S}_{Ref}] * [S_{Sample}(i) - \bar{S}_{Sample}]}{\left\{\sum [S_{Ref}(i) - \bar{S}_{Ref}]^2\right\} * \left\{\sum [S_{Sample}(i) - \bar{S}_{Sample}]^2\right\}}, \quad (1)$$

where $S_{ref}(i)$ is the normalized intensity at position i of the reference spectrum, $S_{sample}(i)$ is the normalized intensity at position i of the sample spectrum, $\bar{S}_{ref}$ is the mean intensity value of the

normalized reference spectrum and $\bar{S}_{sample}$ is the mean intensity value of the normalized sample spectrum.

The resulting correlation coefficient map of the image is built on the spectral information in the sample and is therefore based on dye distribution. Hereby, the highest CC value of one represents complete accordance between sample and reference spectrum. Decreasing CC values indicate decreasing correlation of the spectra.

To enable a comparison of the different images, the uptake indicator UI_x is introduced. It represents the quantity of coefficients higher than a threshold normalized to the total number of pixels representing tissue.

$$UI_x = \frac{\text{Number of correlation coefficients higher } x}{\text{Number of tissue pixels}} \quad (2)$$

These tissue pixels are derived by calculating the standard deviation of the normalized spectral data for every pixel. A uniformly distributed intensity profile along the λ-axis indicates background pixels that are not included in the calculations.

Because UI_x depends on an arbitrary threshold, two evaluation experiments were carried out. In the first experiment untreated skin samples were used to calculate the fraction that is false positively classified as Nile Red pixels with increasing threshold values (see Table 1).

Table 1 indicates the fraction of pixels of an untreated skin sample that are false positively calculated to be similar to the dye reference spectrum.

In the second experiment the reference skin samples were used to evaluate the highest threshold that allows a clear discrimination between the used concentrations.

Figure 4 shows the results of the reference samples indicating that $UI_{0.9}$ is not suitable to allow discrimination of the two lowest concentrations, whereas it is possible when using $UI_{0.8}$. Considering the very low false positive classification of. 02%, $UI_{0.8}$ was used as the evaluation parameter for further experiments.

2.8 *Validation Measurements*

To confirm that the scheme is not depending on absolute intensity values, the samples were imaged with different intensification by varying photomultiplier (PMT) voltages in a range from 500 V to 1200 V in eight steps. $UI_{0.8}$ was calculated for every image and was expected to be constant for different image intensity levels. For the second experiment the focal depth was changed during imaging of two skin samples and $UI_{0.8}$ was calculated to assess the influence of focusing.

Table 1 Measurements of untreated skin samples ($n = 5$) for the evaluation of the 0 parameter.

	$UI_{0.4}$	$UI_{0.5}$	$UI_{0.6}$	$UI_{0.7}$	$UI_{0.8}$	$UI_{0.9}$
Mean (%)	3.6	.9	.4	.09	.02	.0002
StdDev (%)	.9	.4	.1	.03	.01	.0002

Table 2 Presentation of the skin penetration results in mean $UI_{0.8}$ and standard deviation for the four time periods.

$UI_{0.8}$	3 h	6 h	8 h	24 h
Mean (%)	0.7	1.5	3.0	13.8
StdDev (%)	0.6	1.1	2.6	4.8

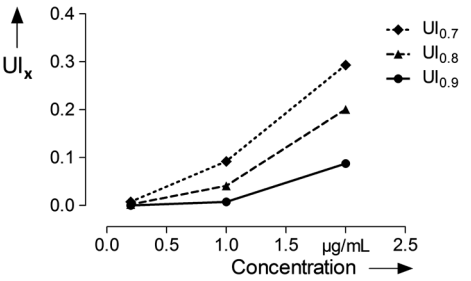

Fig. 4 Determination of the appropriate value for UI_x. The graph shows the $UI_{0.7}$, $UI_{0.8}$ and $UI_{0.9}$ values for 0.2 µg/mL, 1 µg/mL and 2 µg/mL Nile Red reference skin samples. It is not possible to discriminate the 0.2 µg/mL and 1 µg/mL sample when using $UI_{0.9}$.

3 Results

3.1 *Scheme Validation*

The results of the validation experiment for varying signal intensities are shown in Fig. 5(a). Regarding the variation of the PMT voltage to modify the image intensity, $UI_{0.8}$ is nearly constant over a 200 to 300 V region for the 24 h and 8 h samples. The $UI_{0.8}$ increase at 500 to 600 V can be explained with the very low overall intensity of the spectral images at 500 V. Thus, the spectra cannot be properly measured. The $UI_{0.8}$ decrease starting at 900 to 1000 V can be observed due to a strong signal saturation effect in single spectral bands for the 8 h and 24 h samples. Therefore, the spectral information is lost because of detector saturation. The 6 h sample has a $UI_{0.8}$ value that is constant over the range of 600 to 1200 V.

These measurements indicate that the $UI_{0.8}$ values do not change significantly over a broad intensity interval when using reasonable imaging parameters.

Focus position, in contrast, is a very sensitive parameter. The graph in Fig. 5(b) shows a Gaussian-like distribution of $UI_{0.8}$ with varying focus depths for the 10 μm thick sample. The measurements indicate that it is important to focus carefully for getting reliable results. Considering the moderate $UI_{0.8}$ change around the -1 µm to 1 μm relative focus position, a roughly 3-μm tolerance margin for focusing can be supposed.

3.2 *Skin Penetration Study*

The results of the penetration study show a strong time dependence of dye uptake in skin (see Fig. 6 and Table 2). The assessment of this uptake using the $UI_{0.8}$ parameter allows the quantitative comparison of the four time periods. It shows that the 24 h samples have a more than four times higher mean $UI_{0.8}$ value compared to the 8 h samples.

The overlay intensity-based images and the spectrally resolved dye distribution are shown in Fig. 7. The intensity-based images were recorded with optimized parameters to achieve high image quality. The dye distribution was visualized using the correlation coefficient map and the $UI_{0.8}$ parameter as a threshold. The epidermal skin layer can be distinguished from the lower dermal layer due to its bright gray appearance. The

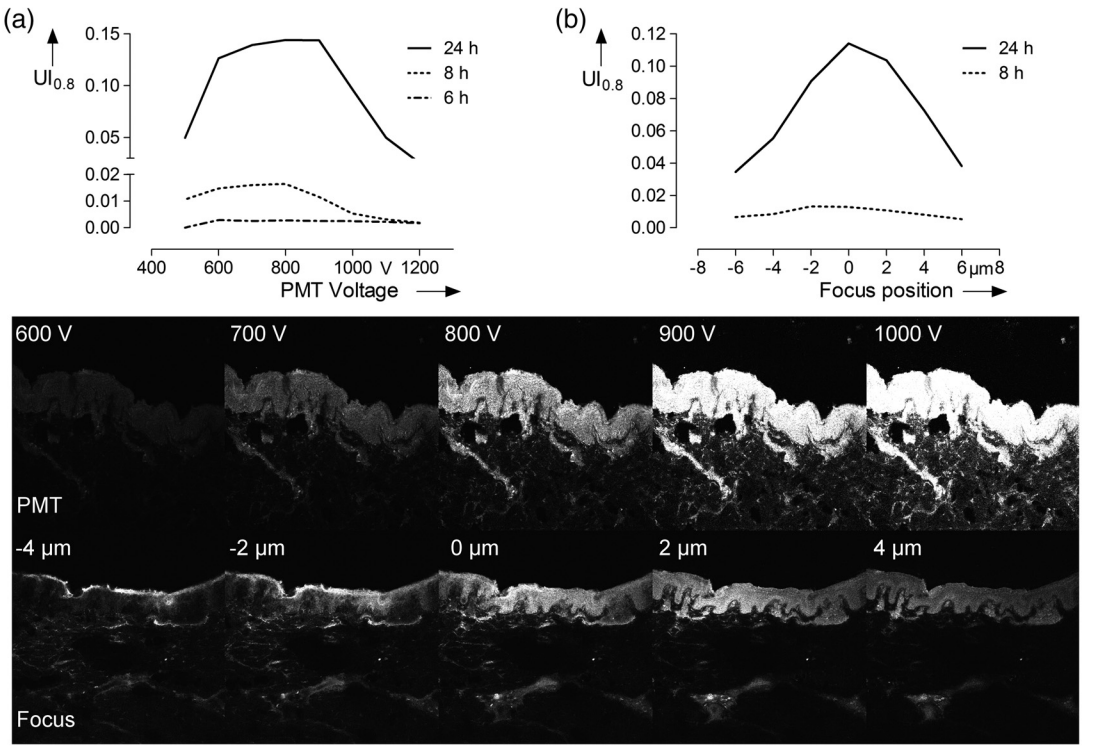

Fig. 5 The graphs show the results of the varying PMT (a) and focus (b) settings. The image sequences illustrate the changes in the data when varying the PMT voltage and the focus depth, respectively.

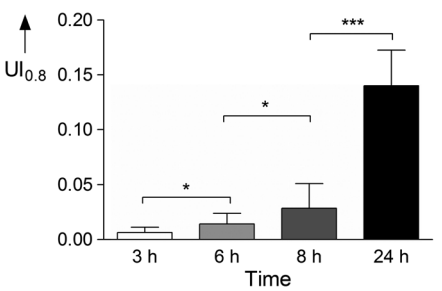

Fig. 6 Skin penetration study results ($n = 20$ per penetration period). Data are presented in mean ±SD. $^{*}P < 0.05$ and $^{***}P < 0.001$ evaluated by paired Student's *t*-test. The 24 h samples show a significantly higher uptake of Nile Red.

darker dermal layer, however, shows brighter structures throughout the whole area. Dye distribution, shown in red, indicates that for the 3 h, 6 h and 8 h samples, the uptake does not cover the whole epidermis in the way that the $UI_{0.8}$ criteria is fulfilled. The 24 h sample shows complete uptake in the epidermis and additional uptake in the dermis layer.

4 Discussion

It was shown that a spectrally resolved imaging and processing method can be used to assess and compare spectral information in tissue. The processing scheme calculates the introduced uptake indicator that derives from spectral correlation analysis. It can be used for mapping spectral information in microscopic images of tissue. The method is developed and validated in the context of a very frequently performed penetration experiment according to the OECD Guidelines for Testing of Chemicals in pharmaceutical research. However, the scope of the method is not limited to drug delivery studies but can be transferred to further applications that need spectral discrimination at a microscopic scale.

4.1 *Pharmaceutical In Vitro Experiments*

High dermal transport is important to address skin diseases occurring in the upper layers. Tape-stripping methods are commonly used to stepwise ablate small parts of the outer skin for quantitatively analyze depth profiles.[29] However, it is limited to the stratum corneum and does not give any information of the homogeneity and the distribution of drugs in the skin layer itself. In contrast, microscopic evaluation of vertical slices has the capability to show profiles directly throughout the whole skin, but lacks the possibility to quantify the amount of penetrated substances. Schmidts[30] presented a skin penetration study that correlated an ELISA based quantification with an intensity-based microscopy evaluation method. The results were of good qualitative accordance indicating the suitability of the microscopy approach for evaluating dermal delivery systems. The developed uptake indicator of this paper was a consequent advancement of Schmidts' microscopy analysis. It allows indirect quantitative measurements and is a step towards the quantitative evaluation of dermal delivery systems and processes. The results of the presented penetration study support this statement as they show a clear discrimination of the four time periods.

Our proposed method may also be beneficial to studies involving applications of spectral and hyperspectral imaging of penetration studies. Roberts; et al.; performed delivery studies using a FLIM multiphoton system[4] that is capable of spectrally detecting fluorescence signal to compare liposome systems. They concluded that the deformability of the liposomes increases penetration based on visual evaluation. In this case, the uptake

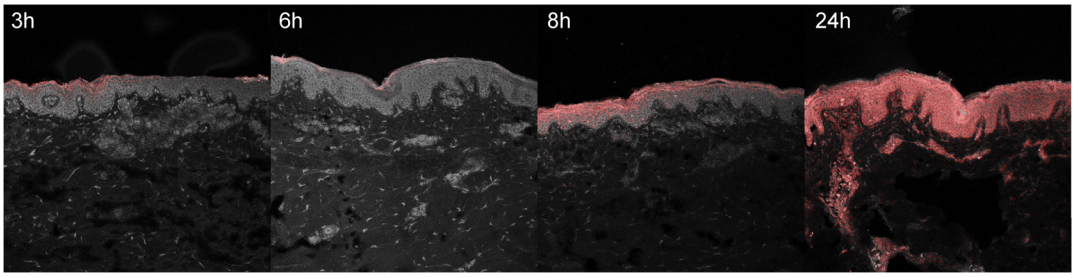

Fig. 7 Overlay of the intensity based confocal images of the skin and the spectrally resolved dye distribution (shown in red, please refer to the online version of this manuscript) for the four time periods.

indicator could be used to obtain comparable results and further increase insight into underlying penetration processes.

Hernandez-Palacios[14] introduced a hyperspectral camera system with 20 μm spatial resolution to evaluate penetration studies. The hyperspectral camera detected the emission peak of Alexa 488 (518 to 524 nm) and therefore avoided the use of fluorescence filters. However, the evaluation is based on the fluorescence intensity that is composed of Alexa dye and skin autofluorescence background. Skin structures like melanin and keratin, with an emission peak at 520 nm,[2,4] contribute to this intensity. Subtraction of a constant offset value compensates the overlaying signal. Figure 7 illustrates that, when using microscopic resolution, structures of the skin are brightly visible that are not covered with dye. In this case, the overlapping and superimposing signal of the skin and dye vary depending on microscopic structures that are not equally distributed. Hence, a constant autofluorescent background offset cannot be defined and mapping of the dye based on intensity in the microscopic scale is not possible.

4.2 *Advantages and Drawbacks for Delivery Studies*

The spectral imaging scheme has several benefits. Additional to the advantage of accurate dye mapping, spectral analysis is superior to intensity-based methods in terms of experiment procedures because it does not require standardized imaging. In general, the emission intensity in confocal microscopy depends on various parameters. Therefore, when using intensity-based methods, it is a comprehensive but very important task to use constant settings in order to assure the comparability of the results. This standardization process requires the assessment and control of imaging setup and sample conditions. While the setup may be kept constant for a whole experiment with certain effort, the sample conditions cannot be controlled easily due to their biological nature.

It is known that the pH-value changes in different skin layers[31] and may influence the intensity of dyes that have a strong pH-dependency. Apart from the pH value, fluorescence emission can also be affected by polarity. In the case of Nile Red, the fluorescence is unaffected by pH-values between 4.5 and 8.5 but the emission peak shifts depending on the polarity of the environment.[25] A possible shift must be considered for choosing the appropriate reference spectrum for image processing calculations. Additionally, photobleaching is a serious problem that requires attention. Borgia[6] reports a 4 to 16% bleaching rate after a one second illumination of Nile Red. It is concluded that the images have to be taken within 10 ms to avoid a strong signal variation.

The spectral data do not depend on absolute intensity values but on relative intensity changes between single wavebands. Consequently they are less sensitive to condition variations and photobleaching resulting in a high robustness of the calculated results. Figure 5 shows that the calculated assessment parameter is constant for reasonable changes of the imaging parameters. This allows measuring every sample with individual settings without the need to use standardized imaging parameters for comparing the results. The advantage is a broad, analyzable concentration range of fluorescent dye in skin specimens. This is especially useful for comparing completely independent experiment setups.

Another advantage of the spectral method is that it is still applicable whenever dyes with emission spectra that are clearly separated from the skin spectrum are not available. Although the spectra overlap, an explicit correlation to either dye or tissue can still be performed. As a result, a reliable assessment of the spatial distribution of dye in tissue is possible.

The $UI_{0.8}$ parameter that is chosen for the evaluation of the penetration study is an arbitrary measure. It is important to understand that it cannot be used to quantitatively assess the total amount of dye in skin. Due to the overlapping dye and skin spectra, it is difficult to determine the exact correlation coefficient that describes the transition between the two possible signal origins. The $UI_{0.x}$ parameters are used to arbitrarily classify the calculation results into dye and tissue pixels according to a threshold value. For this reason the proposed spectral method is not applicable for tasks that need exact quantitative results. In these cases intensity-based methods can be used that need to be calibrated or intensity corrected. Monte Carlo simulations that determine and compensate for effects of signal attenuation due to scattering and absorption[32] are often applied for these applications. Combining these techniques with the spectral evaluation for penetration studies would add valuable information to the localization and penetration depth of dye and agents.

4.3 *Pharmaceutical In Vivo Experiments*

It is arguable that *in vitro* results can be used to assess delivery systems designed for *in vivo* use. No clear data is available in the literature as there are many studies with good and poor correlation between *in vitro* and *in vivo* results.[33] Therefore, *in vitro* results for drug delivery cannot be transferred directly to *in vivo* considerations without further investigation. For this reason, studies are performed with a parallel *in vivo/in vitro* setup[34–36] using living mice for the application and penetration of delivery systems and substances. The mice either are sacrificed or biopsies are taken for analysis afterwards. An approach

for *in vivo* imaging without sacrificing the animals is the use of animal window models.[37,38] Here, the living animal can be microscopically examined directly through windows that are surgically inserted into the region of interest. Whenever living animals are observed motion artifacts have to be considered and either fixation or synchronizing the scanning system to the heartbeat needs to be performed. Amornphimoltham[39] reviewed further *in vivo* applications for drug delivery research and showed the technical efforts that have to be made for data acquisition.

4.4 *Feasibility for Clinical In Vivo Applications*

Gareau[40] presented an approach of *in vivo* confocal reflectance microscopy for the detection of early-stage melanoma of murine skin without further surgical interventions. Lange-Asschenfeld[41] and Caspers[42] showed confocal laser-scanning microscopes for *in vivo* imaging of human skin morphology and wound healing. Both studies mention the potential use for pharmaceutical research on drug delivery. A combination of the proposed microscope setup and our spectrally resolved detection unit could be used for optical sectioning and evaluation of fluorescent dyes in living tissue. Additionally, the *in vivo* microscopy scheme presented by Gareau combined with our proposed spectral uptake indicator could be used in clinical applications like melanoma detection presented by Kuzmina[15] for monitoring size and shape variations.

Extending established microscopic *in vivo* imaging schemes with our proposed spectral evaluation method has the chance to provide additional information for pharmaceutical and clinical applications. However, further investigation is necessary to validate these potential approaches.

Acknowledgments

We would like to thank the Hessen State Ministry of Higher Education, Research and the Arts for the financial support within the Hessen initiative for scientific and economic excellence (LOEWE-Program).

References

1. R. Alvarez-Román et al., "Visualization of skin penetration using confocal laser scanning microscopy," *Eur. J. Pharm. Biopharm.* **58**(2), 301–316 (2004).
2. K. Schenke-Layland et al., "Two-photon microscopes and in vivo multiphoton tomographs—powerful diagnostic tools for tissue engineering and drug delivery," *Advanced Drug Delivery Reviews* **58**(7), 878–896 (2006).
3. S.-J. Lin, S.-H. Jee, and C.-Y. Dong, "Multiphoton microscopy: a new paradigm in dermatological imaging," *Eur. J. Dermatol.* **17**(5), 361–366 (2007).
4. M. S. Roberts et al., "Non-invasive imaging of skin physiology and percutaneous penetration using fluorescence spectral and lifetime imaging with multiphoton and confocal microscopy," *Eur. J. Pharm. Biopharm.* **77**(3), 469–488 (2011).
5. H. I. Labouta et al., "Combined multiphoton imaging-pixel analysis for semiquantitation of skin penetration of gold nanoparticles," *Int. J. Pharm.* **413**(1–2), 279–282 (2011).
6. S. L. Borgia et al., "Lipid nanoparticles for skin penetration enhancement-correlation to drug localization within the particle matrix as determined by fluorescence and parelectric spectroscopy," *J. Contr. Release* **110**(1), 151–163 (2005).
7. M. R. Prausnitz and R. Langer, "Transdermal drug delivery," *Nat. Biotechnol.* **26**(11), 1261–1268 (2008).
8. P. L. Honeywell-Nguyen and J. A. Bouwstra, "Vesicles as a tool for transdermal and dermal delivery," *Drug Discov. Today Tech.* **2**(1), 67–74 (2005).
9. R. H. H. Neubert, "Potentials of new nanocarriers for dermal and transdermal drug delivery," *Eur. J. Pharm. Biopharm.* **77**(1), 1–2 (2011).
10. M. Kreilgaard, "Influence of microemulsions on cutaneous drug delivery," *Advanced Drug Delivery Reviews* **54**(Suppl. 1), S77–S98 (2002).
11. M. Kreilgaard, E. J. Pedersen, and J. W. Jaroszewski, "NMR characterisation and transdermal drug delivery potential of microemulsion systems," *J. Contr. Release* **69**(3), 421–433 (2000).
12. M. J. Lawrence and G. D. Rees, "Microemulsion-based media as novel drug delivery systems," *Advanced Drug Delivery Reviews* **45**(1), 89–121 (2000).
13. T. W. Prow et al., "Nanoparticles and microparticles for skin drug delivery," *Advanced Drug Delivery Reviews* **63**(6), 470–491 (2011).
14. J. Hernandez-Palacios et al., "Hyperspectral characterization of fluorophore diffusion in human skin using a sCMOS based hyperspectral camera," *Proc. SPIE* **8087**, 808717 (2011).
15. I. Kuzmina et al., "Towards noncontact skin melanoma selection by multispectral imaging analysis," *J. Biomed. Opt.* **16**(6), 060502 (2011).
16. S.-G. Kong, "Inspection of poultry skin tumor using hyperspectral fluorescence imaging," *Proc. SPIE* **5132**, 455–463 (2003).
17. M. S. Chin et al., "Hyperspectral imaging for early detection of oxygenation and perfusion changes in irradiated skin," *J. Biomed. Opt.* **17**(2), 026010 (2012).
18. L. L. Randeberg, "Hyperspectral imaging of bruised skin," *Proc. SPIE* **6078**, 60780O (2006).
19. L. L. Randeberg et al., "In vivo hyperspectral imaging of traumatic skin injuries in a porcine model," *Proc. SPIE* **6424**, 642408 (2012).
20. J. M. Beach, "Portable hyperspectral imager for assessment of skin disorders: preliminary measurements," *Proc. SPIE* **5686**, 111–118 (2005).
21. B. Park et al., "AOTF hyperspectral microscopic imaging for foodborne pathogenic bacteria detection," *Proc. SPIE* **8027**, 802707 (2011).
22. R. Arora, G. I. Petrov, and V. V. Yakovlev, "Hyperspectral coherent anti-Stokes Raman scattering microscopy imaging through turbid medium," *J. Biomed. Opt.* **16**(2), 021116 (2011).
23. G. N. Stamatas and N. Kollias, "In vivo documentation of cutaneous inflammation using spectral imaging," *J. Biomed. Opt.* **12**(5), 051603 (2007).
24. C. Zakian et al., "In vivo quantification of gingival inflammation using spectral imaging," *J. Biomed. Opt.* **13**(5), 054045 (2008).
25. D. L. Sackett and J. Wolff, "Nile red as a polarity-sensitive fluorescent probe of hydrophobic protein surfaces," *Anal. Biochem.* **167**(2), 228–234 (1987).
26. D. I. Friedman, J. S. Schwarz, and M. Weisspapir, "Submicron emulsion vehicle for enhanced transdermal delivery of steroidal and nonsteroidal antiinflammatory drugs," *J. Pharm. Sci.* **84**(3), 324–329 (1995).
27. T. Schmidts, "Protective effect of drug delivery systems against the enzymatic degradation of dermally applied DNAzyme," *Inter. J. Pharm.* **410**(1–2), 75–82 (2011).
28. C. Herkenne et al., "Pig ear skin ex vivo as a model for in vivo dermatopharmacokinetic studies in man," *Pharm. Res.* **23**(8), 1850–1856 (2006).
29. J. Lademann et al., "The tape stripping procedure—evaluation of some critical parameters," *Eur. J. Pharm. Biopharm.* **72**(2), 317–323 (2009).
30. T. Schmidts et al., "Development of drug delivery systems for the dermal application of therapeutic DNAzymes," *Inter. J. Pharm.* **431**(1–2), 61–69 (2012).
31. H. Wagner et al., "pH profiles in human skin: influence of two in vitro test systems for drug delivery testing," *Eur. J. Pharm. Biopharm.* **55**(1), 57–65 (2003).
32. U. Maeder, "Feasibility of Monte Carlo simulations in quantitative tissue imaging," *International Journal of Artifical Organs* **33**(4), 253–259 (2010).
33. B. Godin and E. Touitou, "Transdermal skin delivery: predictions for humans from in vivo, ex vivo and animal models," *Advanced Drug Delivery Reviews* **59**(11), 1152–1161 (2007).
34. Z.-R. Huang et al., "In vitro and in vivo evaluation of topical delivery and potential dermal use of soy isoflavones genistein and daidzein," *Inter. J. Pharm.* **364**(1), 36–44 (2008).

35. F. C. Rossetti, "A delivery system to avoid self-aggregation and to improve in vitro and in vivo skin delivery of a phthalocyanine derivative used in the photodynamic therapy," *J. Contr. Release* **155**(3), 400–408 (2011).
36. M. E. M. J van Kuijk-Meuwissen et al., "Application of vesicles to rat skin in vivo: a confocal laser scanning microscopy study," *J. Contr. Release* **56**(1–3), 189–196 (1998).
37. M.-A. Abdul-Karim et al., "Automated tracing and change analysis of angiogenic vasculature from in vivo multiphoton confocal image time series," *Microvascular Research* **66**(2), 113–125 (2003).
38. S. Schlosser et al., "Paracrine effects of mesenchymal stem cells enhance vascular regeneration in ischemic murine skin," *Microvasc. Res.* **83**(3), 267–275 (2012).
39. P. Amornphimoltham, A. Masedunskas, and R. Weigert, "Intravital microscopy as a tool to study drug delivery in preclinical studies," *Advanced Drug Delivery Reviews* **63**(1–2), 119–128 (2011).
40. D. S. Gareau et al., "Noninvasive imaging of melanoma with reflectance mode confocal scanning laser microscopy in a murine model," *J. Investig. Dermatol.* **127**(9), 2184–2190 (2007).
41. S. Lange-Asschenfeldt et al., "Applicability of confocal laser scanning microscopy for evaluation and monitoring of cutaneous wound healing," *J. Biomed. Opt.* **17**(7), 076016 (2012).
42. P. J. Caspers, G. W. Lucassen, and G. J. Puppels, "Combined in vivo confocal Raman spectroscopy and confocal microscopy of human skin," *Biophys J.* **85**(1), 572–580 (2003).